FINAL TECHNICAL REPORT

U.S. Geological Survey
National Earthquake Hazards Reduction Program

Award Number G20AP00078

Paleoseismic and seismotectonic investigations of the Black Butte–San Joaquin faults system as proximal seismic sources to the Sacramento–San Joaquin Delta: Collaborative Research with the U.S. Geological Survey

by

Yann Gavillot[1,2] and Andrew Meigs[2]

[1]Montana Bureau of Mines and Geology, Montana Technological University
1300 W. Park Street, Butte, MT 59701
Email: ygavillot@mtech.edu; Phone: (406) 496-4890

[2]College of Earth, Ocean, and Atmospheric Sciences, Oregon State University
104 Admin Building, Corvallis, OR 97331

Term of Award:
May 15, 2020 – September 30, 2021

Research supported by the U.S. Geological Survey (USGS), Department of the Interior, under USGS award number G20AP00078. The views and conclusions contained in this document are those of the authors and should not be interpreted as representing the opinions or policies of the U.S. Geological Survey. Mention of trade names or commercial products does not constitute their endorsement by the U.S. Geological Survey.

ABSTRACT

The Black Butte–San Joaquin faults system are transpressional faults with late Quaternary-Holocene surface folding and fault scarps. No earthquake history exists for the Black Butte–San Joaquin faults, in spite of the fact that they could pose strong shaking hazard to the nearby heavily populated Sacramento–San Joaquin Delta in Northern California. New age data from our Corral Hollow paleoseismic trench site document at least 4 surface rupturing earthquakes since ~13 ka. OxCal Bayesian modeling of 20 radiocarbon ages constrain the timing of earthquakes E1–E4 in context of stratigraphic and structural relations of fault-scarp derived colluvial wedges. Black Butte fault earthquakes occurred at ~1 ka (E1), ~ 3 ka (E2), ~11 ka (E3), and ~13 ka (E4). Estimates of earthquake intervals range between ~2 ka and ~8 ka, with a preferred recurrence interval of ~2 ka. A vertical slip deficit of ~0.8–1.4 m since the last earthquake (ca. 1 ka) suggests multiple earthquakes or a single large event are needed to relieve accumulated interseismic strain via ~0.2–0.5 m slip-per event. Our results indicate the Black Butte–San Joaquin faults system has the potential to generate significant surface rupture earthquakes. Each individual segment of the Black Butte and San Joaquin faults are at minimum ~30 km-long. Along strike, the San Joaquin fault extends ~85 km to the southeast along the mountain front. The Black Butte and San Joaquin faults could generate Mw ~6.2–6.8 to Mw ~7.2–7.3 reverse-fault earthquakes, respectively. Such earthquakes and associated ground shaking on the Black Butte-San Joaquin fault system likely would affect the greater Delta region including critical water infrastructure including levee systems, canals, and pipelines.

1. INTRODUCTION

The Sacramento–San Joaquin Delta is a nexus of California's water delivery infrastructure and contains extensive vulnerable agricultural, ecological, and water resources (Fig. 1). Earthquake ground shaking damage could have profound consequences for the greater Delta region including flooding and land subsidence that can compromise the levees, canals, pipelines, and aqueducts. Seismic sources are recognized from the well-known major active faults further west in the San Francisco Bay Area such as the San Andreas fault, Hayward fault, and Calaveras fault (e.g., UCERF3; Field et al., 2013). On the other hand, Quaternary faults in the Delta are either not included or not well constrained in existing hazard analyses. These faults close the Delta, many of which are reverse faults, potentially pose larger seismic hazards associated with strong earthquake ground shaking relative to Bay Area strike-slip faults farther to the west (Fig. 1).

Earthquake history, fault geometry, and slip rates for many of the Quaternary faults near the Delta are unknown, which hampers our ability to constrain earthquake potential and recurrence for improved seismic hazard assessments. Delta faults, particularly blind reverse or thrust faults have poorly defined fault or fold scarps, low slip rates, and little to no measurable seismicity. Some of the fault segments associated with the Great Valley thrust system, however, have produced damaging earthquakes. The only know historic earthquake sourced close to the Delta occurred during the 1892 Mw 6.4–6.2 Vacaville-Winters earthquake sequence (O'Connel et al., 2001). Anecdotal accounts suggest the earthquake was widely felt across the Sacramento-San Joaquin Delta with significant damage, although the event pre-dates most infrastructure built following the 1906 San Francisco earthquake. Limited seismic source characterization and seismic reflection profile data suggest the earthquake occurred on a blind thrust ramp with no surface rupture, similar to the strain release associated with the 1985 Mw 6.3 Coalinga earthquake

that occurred along strike further south in the San Joaquin Valley (O'Connel et al., 2001; Guzofski et al., 2007). Pre-historic earthquake occurrence and frequency are unknown for any of Delta faults.

A major risk in the Delta is the close proximity of these faults to its extensive levee system, which are constructed on materials with strong liquefaction susceptibility and vulnerability to strong shaking (e.g., Witter et al., 2006; Real and Knudsen, 2010). In addition, many fault crossing-canals and water pipelines are at risk of physical damage (Fig. 1), including the proposed multi-billion-dollar California WaterFix infrastructure project. Although evidence of fault rupture and earthquake history are not readily deduced for blind faults, emergence of lidar, topographic analyses with detailed geomorphic mapping and Quaternary dating methods, as well as geophysical data have enabled to resolve active fault-related deformation near the Delta (e.g., Unruh and Hector, 1999; Unruh et al., 2009; Unruh and Hitchcock, 2015; Gavillot et al., 2018; Gavillot and Meigs, 2020).

Such new datasets exist on the Black Butte–San Joaquin faults system documenting late Quaternary-Holocene surface folding and fault scarps in proximity to the Delta (Fig. 1; Gavillot et al., 2018; Gavillot and Meigs, 2020), which identified a paleoseismic study site (Fig. 2). These transpressional faults are some of the least understood fault segments associated with the Great Valley thrust system in spite of the fact that they could pose strong shaking hazard to the nearby heavily populated Sacramento–San Joaquin Delta. No earthquake data in the paleoseismological or historical records exist for the Black Butte–San Joaquin faults. A Mw 6.65–6.95 earthquake is forecasted for the San Joaquin fault segment using poorly constrained geologic parameters (UCERF3, Field et al., 2013; see Appendix N, Page et al., 2013). The Black Butte fault is currently not included in regional or national seismic hazards assessments. If simultaneous ruptures would occur on multiple faults that are structurally linked at depth (Black Butte and San Joaquin faults), or potential along strike (Midway fault), the combined rupture length could imply an earthquake potential of Mw >>7 (e.g., Wells and Coppersmith, 1994; Stirling et al., 2013).

In this final technical report, we present new results from a paleoseismic trench investigation on the Black Butte–San Joaquin faults system located near Tracy, CA (Figs. 1 and 2). New age data of multiple Holocene earthquake events and surface rupture history on the Black Butte–San Joaquin faults provide constraints on the earthquake potential as a proximal seismic source to the Sacramento–San Joaquin Delta. Our study builds on the detailed mapping, Quaternary age datasets, structural constraints, and slip rates on the Black Butte–San Joaquin faults system (Sowers et al., 2000; Gavillot et al., 2018; Gavillot and Meigs, 2020).

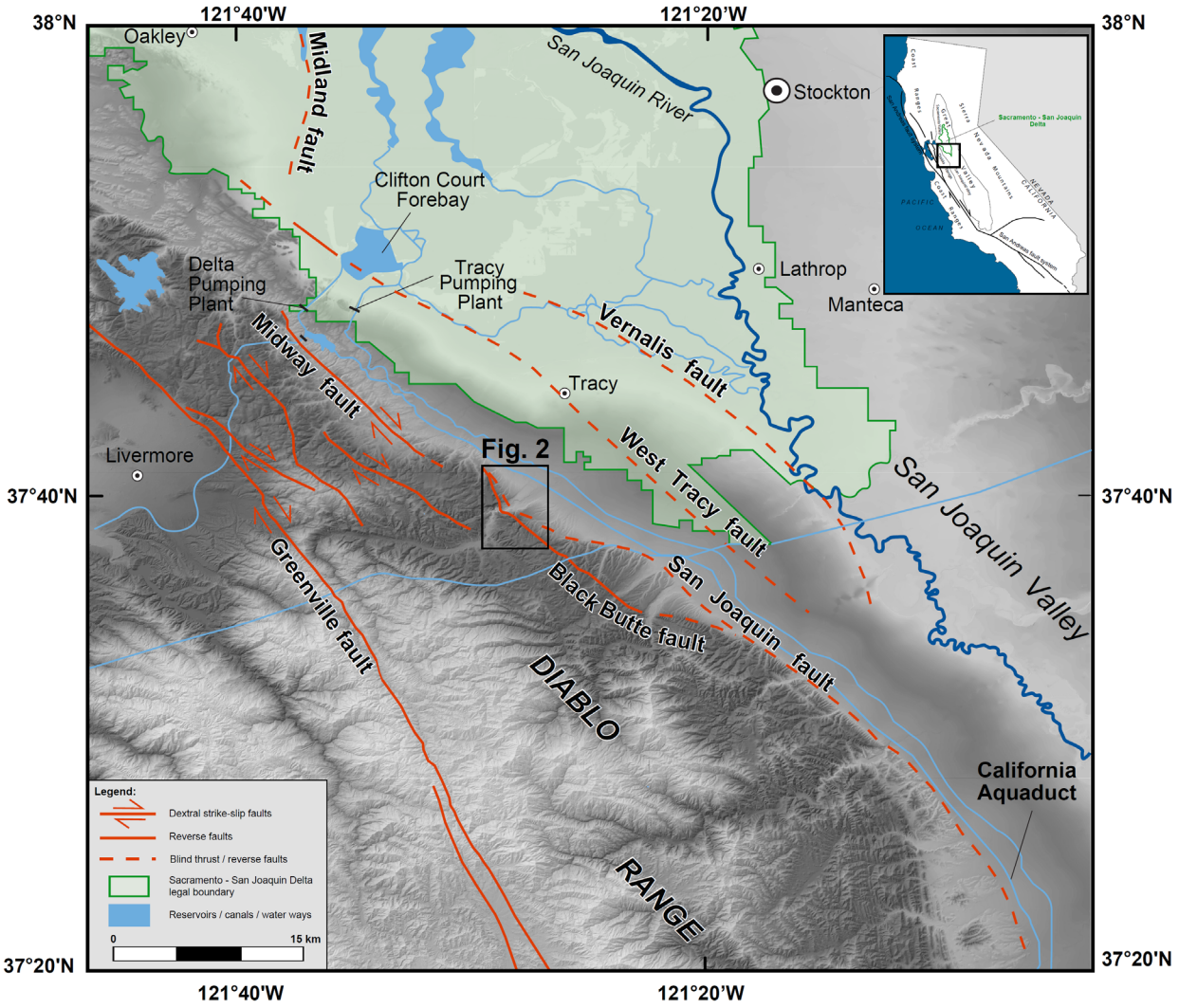

Figure 1. Fault and location map for the southern Sacramento–San Joaquin Delta and Diablo Range with study site shown in Figure 2, modified from Gavillot and Meigs (2020).

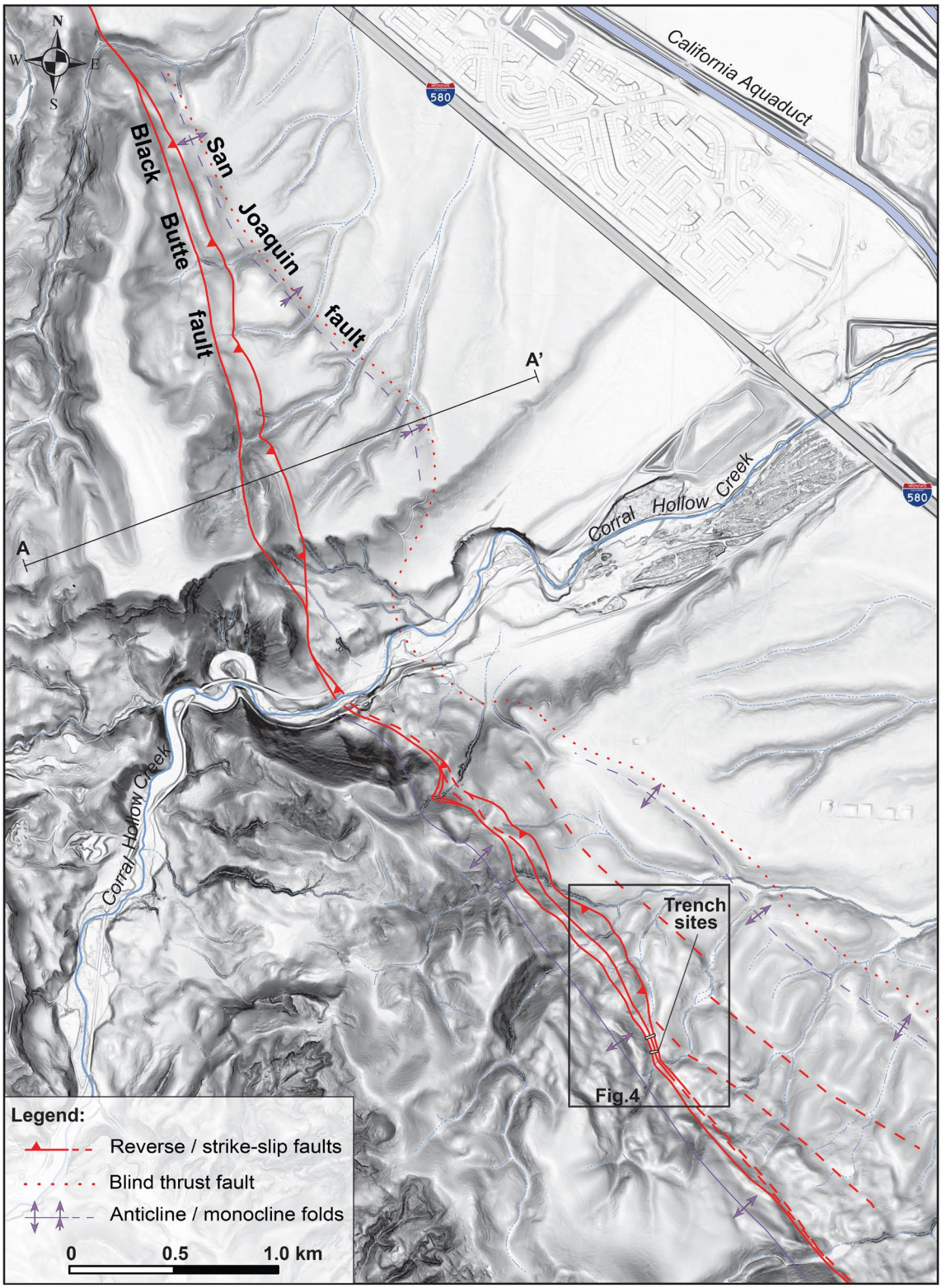

Figure 2. Quaternary fault and fold map of the Black Butte–San Joaquin fault systems at the Corral Hollow study site. Cross section along the transect A–A' is shown in Figure 3. Inset box shows Corral Hollow paleoseismic trench site (Fig. 4). Basemap is 3DEP lidar slopemap.

2. GEOLOGIC SETTING

The southern region of the Sacramento–San Joaquin Delta comprises multiple thrust or reverse fault splays and segments, which include the Black Butte, San Joaquin, West Tracy, and Vernalis faults (Fig. 1; Jennings et al., 1994; Unruh and Krug, 2007; Jennings and Bryant, 2010). The westernmost Black Butte fault is the only structure documented to have fault scarps that offset Pleistocene-Holocene alluvial terraces (Dibblee, 1981; 1981b; Noller et al., 1993; Gavillot et al., 2018; Gavillot and Meigs, 2021). All other faults are inferred to be blind at the same latitude (Fig. 1). Folded alluvial terraces and fold scarps have been interpreted to document Holocene-Pleistocene west-dipping thrust-related deformation above the blind San Joaquin fault along the mountain front (Sowers et al., 2000; Gavillot et al., 2018; Gavillot and Meigs, 2021). The West Tracy fault and Vernalis fault located further east are concealed within the San Joaquin Valley and interpreted as range parallel west-dipping reverse faults based on limited seismic data (Krug et al., 1992; Sterling, 1992; Unruh and Hitchcock, 2015). Further north, the Midway fault (strike-slip fault) and locally West Tracy fault (reverse fault) indicate evidence of near-surface faulting with offset Quaternary surficial deposits and fault scarps (Fig. 1; Dibblee, 1981; 1981b; Unruh and Sawyer, 1995; Unruh and Hitchcock, 2015).

Geomorphic surface age data and slip rates for Delta faults are limited to the Black Butte and San Joaquin faults. A fold scarp along the San Joaquin fault indicate slip rates of 0.15–0.54 mm/yr for 69–24 ka time scale dated by U-series and ^{14}C on carbonate weathering rinds on uplifted alluvial terraces (Sowers et al., 2000). However, a recent study quantified a ~5 km-wide deformation zone across the Black Butte and San Joaquin faults with new detailed mapping and geochronologic datasets of multiple deformed Pio-Pleistocene alluvial fans and Pleistocene-Holocene terrace deposits (Gavillot et al., 2018; Gavillot and Meigs, 2020). Folded and faulted terraces constrain fault activity on the Black Butte–San Joaquin faults system since ~105 ka, with a combined fault slip rate budget of 2.2–3.7 mm/yr and shortening rate of 1.7–3.0 mm/yr (Gavillot and Meigs, 2020). On the West Tracy fault, near the Clifton Court Forebay (Fig. 1), structural relief of Miocene sediments (seismic reflection data), and offset marshland peat deposits (geotechnical borings) yield estimates of separation rates of 0.23–0.34 mm/yr since Neogene to Holocene timescales (Unruh and Hitchcock, 2015). No slip rate estimates exist for the Midway fault or Vernalis fault.

Geodetic data indicate a 1.9–3.5 mm/yr shortening (convergence) rate and a 4.4–5.4 mm/yr dextral strike-slip rate along the western border of the San Joaquin Valley (Prescott et al., 2001; d'Alessio et al., 2005). Rate comparison between available geodetic and geological shortening rates suggest most of the convergence absorbed across the southern Delta region is accounted by Black Butte-San Joaquin faults system (1.7–3.0 mm/yr; Gavillot and Meigs 2020). Other range parallel reverse faults at the same latitude, such as the West Tracy and Vernalis faults may in turn absorb relatively little convergence (<<1 mm/yr). If true, the Black Butte and San Joaquin faults may represent a major fault system in the southern Delta region that accumulate interseismic strain and release via a combination of surface rupture and blind earthquakes. Estimates of dextral strike-slip rates are unknown for the Black Butte–San Joaquin faults system. The Midway fault to the northwest is a likely candidate that absorbs most of dextral strain for the eastern Diablo Range.

3. STRUCTURAL RELATIONS OF THE BLACK BUTTE-SAN JOAQUIN FAULTS

The Black Butte–San Joaquin faults system defines a NW-SE-trending ~30km-long zone of overlapping faults and folds along the eastern Diablo Range mountain front (Figs. 1–2). This fault system extends ~85 km along strike and continues as the San Joaquin fault to the southeast (Fig. 1).

The Black Butte fault (BBF) is a transpressional fault that juxtaposes Cretaceous-Miocene bedrock in its hanging wall against deformed Plio-Pleistocene alluvial fan deposits and overlying fluvial terraces in its footwall. Sequential folding as a fault-bend fold anticline with multiple angular unconformities, and vertically offset Quaternary sediments suggest the BBF has a protracted fault history since the Miocene. Natural exposures, map relations, and structural constraints indicate the BBF is a 40° (± 2°) SW-dipping reverse fault with evidence of oblique to strike-slip motion (Gavillot and Meigs, 2020).

The San Joaquin fault (SJF) is a blind fault that parallels the structural trend of the BBF (Fig. 1). The SJF deforms Plio-Pleistocene to Holocene deposits as a fault-related monocline and anticlinal fold. SJF fault geometry is interpreted as a 30–42° SW-dipping blind thrust based on fold map pattern, cross section constraints, and long-wavelength deformation pattern. The SJF joins the BBF along strike, which suggest the BBF–SJF are fault splays that intersect at depth as structurally and temporally integrated fault system (Gavillot and Meigs, 2020).

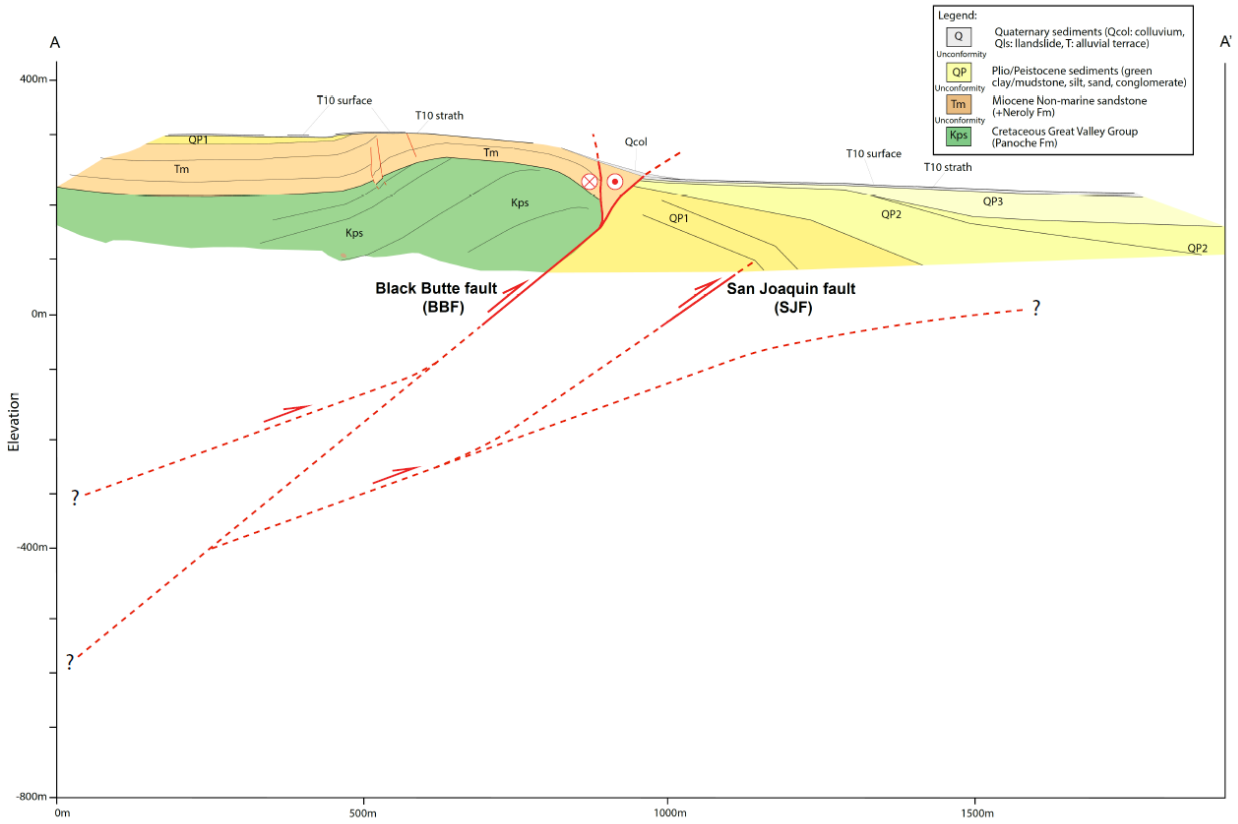

Figure 3. Structural cross section along transect A–A' across Black Butte-San Joaquin faults system at Corral Hollow, modified from Gavillot and Meigs (2020). Transect location is shown in Figure 2.

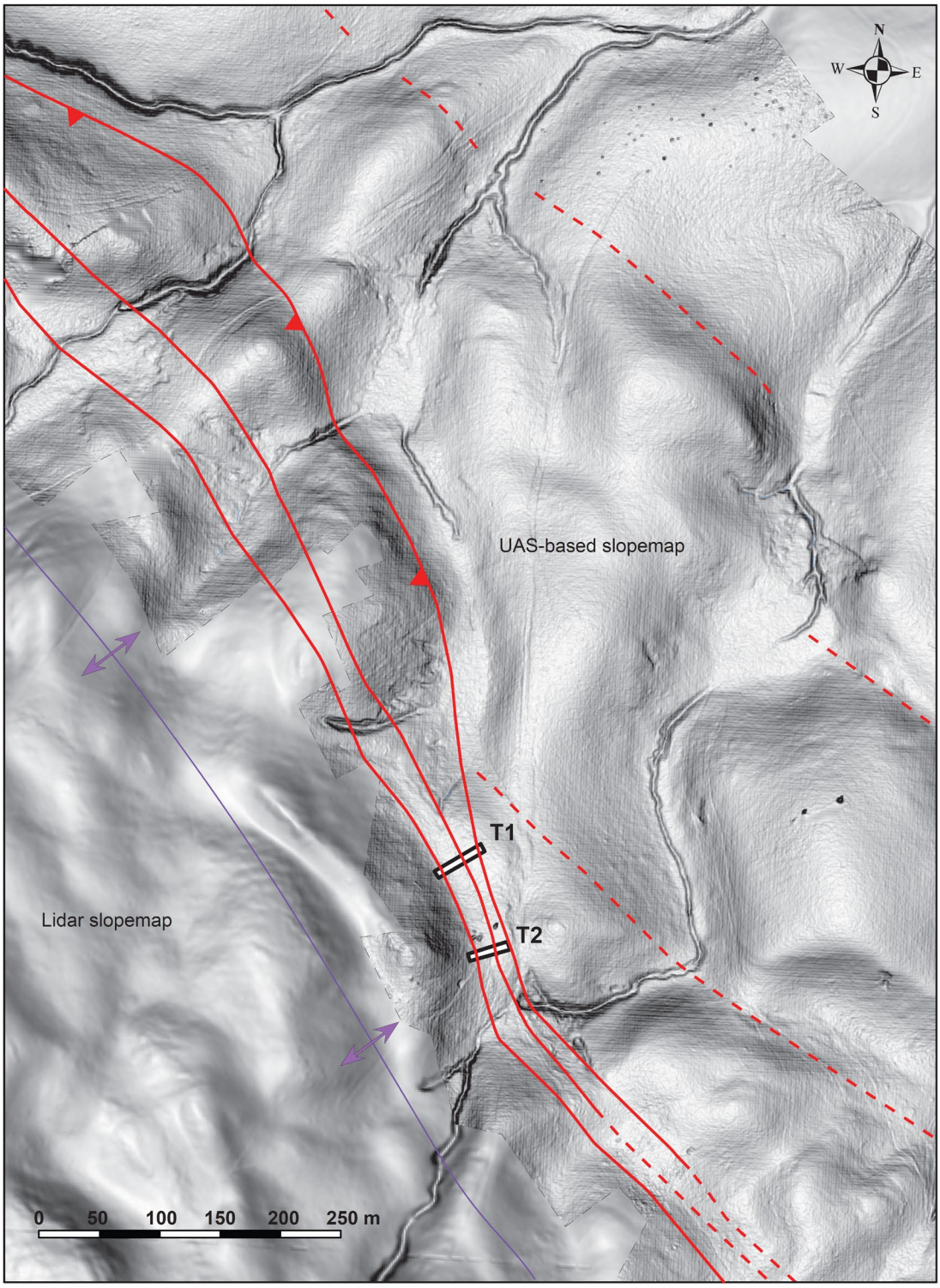

Figure 4. Detailed site map of the Corral Hollow paleoseismic trenches (T1–T2) across multiple strands of the Black Butte fault. Data coverage between UAS (drone)-based slopemap and aerial 3DEP lidar slopemap shown by grey dash lines. T1: Trench 1; T2: Trench 2. Fault symbols are the same as shown in Figure 2.

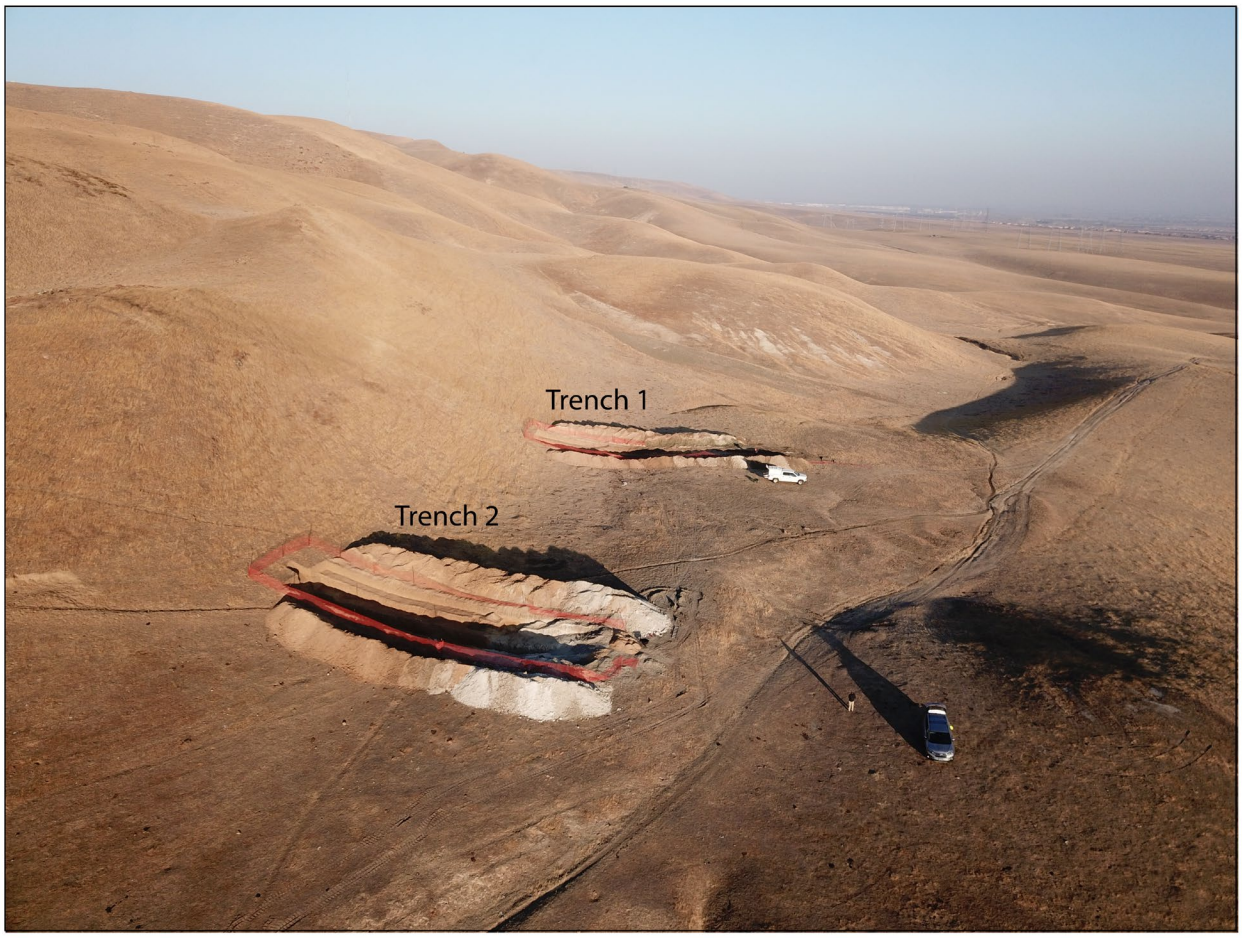

Figure 5. Aerial view looking northwest of the Corral Hollow paleoseismic trenches (T1–T2) excavated across the Black Butte fault (BBF). Scarp at the base of western foothills is the main strand of the (BBF). Light colored ridges and topographic knobs represent structural pop-ups or flower structures associated with the BBF fault splays. Color change in T1 and T2 represent location of faulted Plio/Pleistocene units. Sediments troughs between the BBF main strand and BBF fault splays contain the scarp-derived colluvial wedges.

4. PALEOSEISMIC TRENCH SITE

The study site is located south of Corral Hollow Creek, within the piedmont foothills of the eastern Diablo Range, near Tracy, CA (Fig. 2). The oldest dated alluvial surfaces offset by the BBF in Corral Hollow range between 113 ka and 103 ka based on IRSL and TCN ^{10}Be age data (T10; Fig. 3; Gavillot and Meigs, 2020). Younger fluvial terraces are etched into older Plio-Pleistocene deposits, recognized as regional extensive broad alluvial fans (Tulare Formation; Los Banos Alluvium) and local lacustrine deposits (Corcoran Clay). Map and stratigraphic evidence indicate these alluvial fans deposits represent synorogenic sediments that record sequential deformation associated with BBF-SJF from ~800–600 ka to 211–100 ka (Lettis 1982 and references therein; Lettis and Unruh, 1991; Gavillot and Meigs, 2020).

Topographic steps and east-facing fault scarps define the main fault trace of the BBF (Figs. 2–4). Fault splays of the BBF form linear ridges, saddles, east and west facing scarps, and ponded

sediments in local troughs perched above active creeks. Our Corral Hollow trench site was chosen to target these perched sediment troughs because they potentially preserve colluvial wedges, sag pond deposits, buried soils, and paleochannel deposits structurally bounded by the main BBF fault trace and its footwall fault splays (Fig. 4).

5. METHODOLOGY

Trenching

We employed paleoseismic trenching and surveying techniques to excavate two trenches (T1-T2; Figs. 4–5). Excavation targeted fault segments identified from our mapping. Trench wall exposures were cleaned and photographed. Orthophoto mosaic photogrammetry techniques using Structure from Motion provided high-resolution photo logs generated using Photoscan Metashape software. Stratigraphic and structural relations were traced and described in the trench photo logs. Samples were tagged and collected in the trench walls for geochronological constraints of key stratigraphic units and buried soils using radiocarbon (^{14}C) and infrared stimulated luminescence (IRSL). We used UAV-based photogrammetry to generate detailed georeferenced 3-D site map of the trench locations, faults, and surface geomorphology (Fig. 4).

Quaternary dating

We employed a combination of radiocarbon dating and infrared stimulated luminescence (IRSL) to date silt rich alluvium, buried soils, and colluvial wedges exposed in the paleoseismic trenches. These age results were used to constrain earthquake events.

For ^{14}C dating methodology, we collected multiple samples from detrital charcoal and bulk soil radiocarbon measurements, at successive stratigraphic depth intervals where available to constrain ages of the deposits. These materials were submitted and processed by Susan Zimmerman at the Center for Accelerator Mass Spectrometry (CAMS) of the Lawrence Livermore National Laboratory (LLNL) and Linda Cummings at the PaleoResearch Institute. Submitted samples were chemically pretreated, converted to carbon dioxide and reduced to graphite. Radiocarbon samples that underwent $\delta^{13}C$ analysis when available had an aliquot of carbon dioxide and reported in standard per mil notation. Uncalibrated radiocarbon results from the AMS measurements are reported as conventional radiocarbon ages (years B.P.), with at least 1-sigma standard deviation error of the analysis (Stuiver and Polach, 1977). All radiocarbon results were converted to calibrated ages using OxCal software by Bronk Ramsey (2009). Earthquake timing are determined using the OxCal Bayesian modeling analysis in the context of stratigraphic and structural relations (Bronk Ramsey, 1995; Bronk Ramsey 2009). See Table 1 for the radiocarbon age results.

Infrared stimulated luminescence (IRSL) targets grain-sized feldspars and polycrystalline quartz. IRSL provided a more suitable dating method as samples contained significant amount of polycrystalline quartz that lack of sensitivity response to optically stimulated luminesce (OSL). Sampling targets included sand- or silt-rich facies associated with surficial deposit most likely to have been reset by sunlight exposure (e.g., Rittenour, 2008; Rhodes, 2011). In the field, samples for IRSL dating were collected by pounding opaque metal pipes into sediment layers and were tightly packed to prevent light exposure and sediment mixing. Samples were sent to Shannon Mahan at the USGS Luminescence Laboratory in Denver for processing to purified feldspar separates. Age data from our IRSL samples are forthcoming and will be included in upcoming

publication of the paleoseismic results from this study. Combination of the age results from ^{14}C and IRSL provide independent dating methods to bracket depositional ages and earthquake events.

TABLE 1. RADIOCARBON AGES FOR CORRAL HOLLOW PALEOSEISMIC TRENCHES

Sample	Lab ID[1]	Type[2]	Trench location[3]	Unit	^{14}C Lab Age (yr. B.P)[4]	Calibrated ^{14}C Age (cal yr. B.P.)[5]	Calibrated ^{14}C Age (cal. ka B.P.)	$\delta^{13}C$ ($^{o}/_{oo}$)[6]
BBF-T2S-1	CAMS-185721	D,C	T2S	C2	9410 ± 40	10628 ± 116	10.6 + 0.1	-25
BBF-T2S-2	CAMS-185722	D,C	T2S	C2	8920 ± 240	10069 ± 586	10.1 + 0.6	-25
BBF-T2S-3*	CAMS-185723	D,C	T2S	C3	9890 ± 35	11289 ± 68	11.3 ± 0.1	-25
BBF-T2S-4	CAMS-186448	D,C	T2S	C2	9820 ± 270	10848 ± 550	10.8 ± 0.6	-25
BBF-T2S-6*	CAMS-185724	D,C	T2S	C2	10145 ± 40	11775 ± 164	11.8 ± 0.2	-25
BBF-TS2-7	CAMS-186449	D,C	T2S	C3S	10010 ± 160	11807 ± 618	11.8 ± 0.6	-25
BBF-TS2-8	CAMS-186450	D,C	T2S	C3S	9890 ± 490	11841 ± 851	11.8 ± 0.9	-25
BBF-TS2-9	CAMS-186451	D,C	T2S	C3	9930 ± 270	11772 ± 707	11.8 ± 0.7	-25
BBF-T2S-10	CAMS-185786	D,C	T2S	C3S	10300 ± 60	12145 ± 316	12.1 ± 0.3	-25
BBF-T2S-12	CAMS-185725	D,C	T2S	C3S	10250 ± 40	12094 ± 334	12.1 ± 0.3	-25
BBF-T2N-2	CAMS-185726	D,C	T2N	C3S	10410 ± 120	12224 ± 398	12.2 ± 0.4	-25
BBF-T2N-15	CAMS-186678	D,C	T2N	7S	4140 ± 40	4679 ± 147	4.7 ± 0.1	-25
BBF-T1S-1*	CAMS-186679	D,C	T1S	3S	1.2046 ± 0.0049^{FAC}	-35 ± 1 (AD 1985)	-0.035 ± 0.001	-25
BBF-T1N-3	CAMS-186680	D,C	T1N	7S	4440 ± 35	5080 ± 202	5.1 ± 0.2	-25
BBF-T2S-BS-3*	PRI-6732	BS,C	T2S	C1S	3360 ± 40	3588 ± 106	3.6 ± 0.1	-25.01
BBF-T2S-BS-4	PRI-6733	BS,C	T2S	C1S	2160 ± 30	2156 ± 150	2.2 ± 0.2	-25.22
BBF-T2S-BS-5	PRI-6734	BS,C	T2S	3S	170 ± 60	154 ± 151	0.15 ± 0.15	-24.12
BBF-T2S-BS-6	PRI-6735	BS,C	T2S	2	720 ± 35	643 ± 79	0.64 ± 0.08	-25.67
BBF-T2S-BS-7	PRI-6736	BS,C	T2S	4	1100 ± 20	1008 ± 51	1.01 ± 0.05	-24.98
BBF-T2S-BS-8	PRI-6737	BS,C	T2S	5	3080 ± 30	3588 ± 106	3.3 ± 0.1	-24.98

[1]Samples processed by the Center for Accelerator Mass Spectrometry (CAMS) at Lawrence Livermore National Lab, and PaleoResearch Institute (PRI).

[2]Sample types included detrital (D) and bulk soil (BS) radiocarbon from charcoal (C). Identification for plant species was either not performed or not possible because of sample size.

[3]Trench location included Trench 2 south wall (T2S), T2 north wall (T2N), Trench 1 south wall (T1S), and Trench 1 north wall (T1N).

[4]Laboratory-reported radiocarbon age in ^{14}C yr before A.D. 1950 (B.P.)

[5]Calibrated age before A.D. 1950 (ca. yr B.P.) determine using OxCal version 4.4.2 (Bronk Ramsey, 2009; Bronk Ram,sey and Lee, 2013; Reimer et al., 2013). Ages and errors are reported to nbearest year, and based on 95% probability. For sample BBF-T1S-1, the negative calibrated age is A.D. 1985 (or 35 years after A.D. 1950).

[6]Measured $\delta^{13}C$ are listed to two decimale places. Assumed δ13C values are according to Stuiver and Polach (Radiocarbon, v. 19, p.355, 1977) when listed without decimal places.

[FAC]Fraction modern carbon for ^{14}C age post A.D. 1950. Lab and calibrated ages determined using CALIBomb software (Reimer and Reimer, 2021) and post-Bomb Calibration data NH Zone 2 (Hua 2009; Hua et al., 2021).

*Indicates samples excluded from OxCal Bayesian age model (see Figure 7).

6. RESULTS

Stratigraphic and structural relations

Paleoseismic trenches T1 and T2 were excavated across the multiple fault strands associated with the BBF (Figs. 4–5). The trenches exposed a series of interfingering colluvial wedges and fine-grained slopewash colluvium deposited in a structurally controlled NW-SE-trending trough that parallels the BBF (Figs. 6–7).

The western hillslopes consist of exhumed Cretaceous-Tertiary sandstone (B1) that are sheared and fractured by sub-vertical SW-dipping bedrock faults. These bedrock faults in B1 correlate to the main trace of the BBF as a reverse fault that locally steepens to a transpressional fault (Fig. 3). Landslide and debris flow deposits (units 9–10), and overlying silt-rich slopewash colluvial deposits (units 3–7) bury the B1 unit with no documented penetrative fault offset (Figs. 6–7). The eastern sections of the trenches expose exhumed Pio-Pleistocene clay beds rich in gypsum mineralization (B2) that are highly sheared and plastically deformed by multiple steep NE to SW-dipping faults. Limited exposures of slickenlines on faults in B2 indicate nearly pure oblique slip motion. Faults in B2 truncate sheared colluvium (SC), Pleistocene alluvial deposits (B3) and younger colluvial wedges (C1–C3). The northeastern and southwestern limits of the

faulted B2 unit exposed in the trenches correlate to the mapped BBF footwall fault splays that structurally control topographic ridges as transpressional pop-up or flower structures (Fig. 3).

Within the depositional trough, the trenches expose multiple sub-vertical faults with penetrative offset across all units except the upper soils (units 1–2) and young silt-rich slopewash colluvium (unit 3). Youngest fault displacement is documented by offset and deformation of unit 4, as well as the basal soil horizon of unit 2. Colluvial wedges (C1–C3) are characterized by scarp-derived angular granule to pebble size clasts composed of distinctive white to grey indurated clay beds locally sourced from B2. In addition, many of the colluvial wedge units have corresponding buried soils indicating that periods of erosion recorded in the scarp-derived deposits were followed by intermittent periods of soil development possibly related to seismic quiescence. Penetrative deformation of the colluvial wedge units and buried soils include sheared clay fabric, rotated clasts, filled fissures, and gypsum to calcic mineralization (T1 and T2; Figs. 6–7).

Earthquake events

The stratigraphic relations and radiocarbon analyses suggest at least 4 surface-rupturing earthquake events occurred since ~13 ka (Table 1; Figs. 7–8). The most recent event, E1, is bracketed by fault offset in unit 4 (~1.0–1.1 cal ka BP) and the overlying undeformed unit 3 (~0.6–0.7 cal ka BP). Older events E2–E4 are constrained by stratigraphic successions of fault-scarp derived colluvial wedges and slopewash colluvium. E2 occurred before deposition of colluvial wedge C1 (~2.0–2.3 cal. ka BP). E3 occurred before deposition of colluvial wedge C2 (~10.1–10.8 cal. ka BP). E4 occurred prior to deposition of colluvial wedge C3 (~11.8–12.2 cal. ka BP).

Bayesian modeling of 20 radiocarbon ages using OxCal (Bronk Ramsey, 2009) establishes the timing of earthquakes E1–E4 in context of the colluvial wedge stratigraphic and structural relations (Fig. 8). The youngest earthquake, E1 occurred at 0.85 ± 0.19 ka, or between 0.66 ka to 1.03 ka at 95% confidence range. E2 occurred at 2.7 ± 0.6 ka, or between 2.2 ka to 3.3 ka at 95% confidence range. E3 occurred 11.2 ± 0.5 ka, or 10.7 ka to 11.7 ka at 95% confidence range. The oldest recorded earthquake, E4 occurred not later than 13.1 ± 1.1 ka, or between 12.0 ka to 14.3 ka at 95% confidence range.

An erosional contact that truncates C2–C3 in Trench 2 is inferred to represent an unconformity possibly recording a data gap in our earthquake chronology (Figs. 6–8). This erosional event is stratigraphically older than unit 7 (~4.7–5.1 ka; Fig. 7), and may pre-date a paleochannel sand (unit 8) that incised a debris flow deposit (unit 10) (Fig. 6). If an additional earthquake is reflected by this unconformity, the event may have occurred between E3 (11.2 ± 0.5 ka) and unit 7 (~4.7–5.1 ka). Landslide and debris flow deposits (units 9–10) provide non-unique inferential evidence of ground motion, although no definitive scarp derived colluvial wedges are preserved at the southwest limit of the trenches (faults in B1; Fig. 6).

Black Butte fault earthquakes E1 (ca. 1 ka), E2 (ca. 3 ka), E3 (ca. 11 ka), and E4 (ca. 13 ka) allow for estimation of mean earthquake recurrence based on the OxCal Bayesian chronologic model. Recurrence interval for E4-E1 has a mean value of ~4 ka, but reflects a broadly distributed earthquake age distribution. The intervals between events are ~2 ka for E1–E2, ~8 ka for E2–E3, and ~2 ka for E3–E4. It is unclear whether these intervals reflect variable slip distribution on the multiple strands of the BBF, variation in the loading cycle, and incomplete event record or other factors affecting earthquake occurrence in time. Alternatively, 1-2 earthquakes may be recorded between E2 and E3, consistent with an erosional contact and stratigraphic data gap between ~10.1–

10.8 ka (C2) and 4.7–5.1 ka (unit 7), as well as buried landslide deposits (Figs. 6–7; Table 1). If we use the time intervals between events E1–E2 and E3–E4 as proxies, the BBF fault has a recurrence interval of ~2 ka.

Slip per event and slip deficit

Estimates of vertical slip per event are poorly constrained, but range from 0.2 m to 0.5 m for E1–E4 (Figs. 6–7). One key challenge to characterizing slip per event is that the colluvial wedges are not laterally continuous across the faults with largest displacements. We use the thickness of the colluvial wedges as a proxy for minimum vertical fault displacement per event. Colluvial wedge C4 is ~0.5 m thick against the fault for slip displacement in E4. Colluvial wedges C3 and C2 are both ~0.4 m thick against the fault for slip displacements in E3 and E2, respectively. Fault displacement during E1 is recorded by highly distributed deformation on multiple offset units accounting to a total of ~0.2 m. Together, the measurements suggest mean slip per event of ~0.4 m. Although many of the faults exposed in unit B2 indicate evidence of strike slip deformation, no lateral strain marker units were identified in the trenches to measure oblique component of slip-per event. Future work in 3-D trenching are needed to resolve strike-slip displacement with earthquake events.

Loading the Black Butte fault with a fault slip rate of 1.3–2.0 mm/yr (Gavillot and Meigs, 2020) over ~1.0 ka interval since the last earthquake recorded at Corral Hollow implies a slip deficit of 1.3–2.0 m for a subsurface fault dip of 40º ± 2 (Fig. 3; Gavillot and Meigs, 2020). However, the Corral Hollow trenches indicate sub-vertical faults characterize the near surface fault dips of the BBF, translating to a vertical slip deficit of 0.8–1.4 m. Combining our measurements of ~0.4 m slip-per event and ~1.1 m slip deficit on the BBF frame the earthquake potential. In one end of the spectrum, variation in earthquake cycle with a temporal cluster of 2–3 moderate surface rupturing earthquakes are needed to relieve accumulated strain via ~0.4 m per-event slip. A single larger earthquake with ~1.1 m of vertical slip could relieve the predicted accumulated strain and slip deficit. We recognized that our estimates of vertical slip-per event based on faulted colluvial wedges in our trenches likely underestimate the total contractional strain absorbed on the BBF. Alternatively, long-term fault slip rates on the BBF may have decreased during the Holocene. A larger degree of strain partitioning in the last ~13 ka via strike-slip deformation could explain decreasing lower values of vertical slip-per event from E4-E1 than inferred from the loading rate.

Each individual segment of the Black Butte and San Joaquin faults are at minimum ~30 km-long. Along strike, the San Joaquin fault extends ~85 km to the southeast along the mountain front (Fig. 1). Empirical scaling relationships indicate that surface fault lengths of the Black Butte and San Joaquin faults could generate Mw 6.2–6.8 and Mw 7.2–7.3 reverse-fault earthquakes, respectively (Stirling et al., 2013). Such earthquakes and associated ground shaking on the Black Butte-San Joaquin fault system could profoundly affect the greater Delta region including critical water infrastructure such as levee systems, canals, and pipelines.

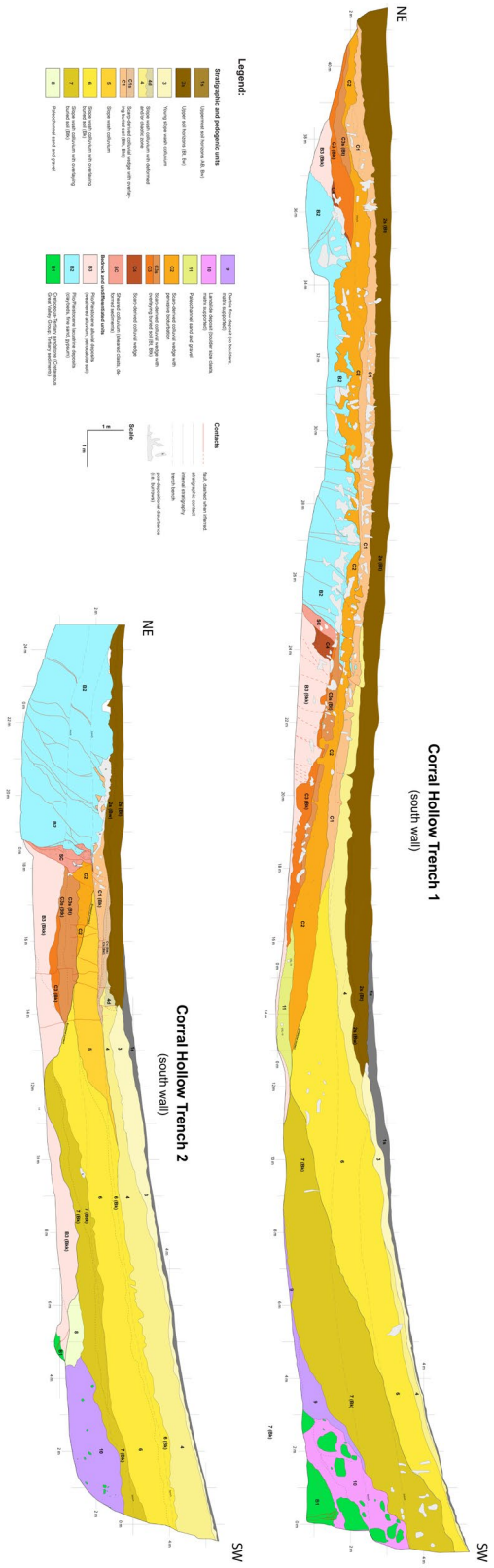

Figure 6. Stratigraphic and structural relations for Trench 1 and Trench 2 south walls of the Corral Hollow paleoseismic site.

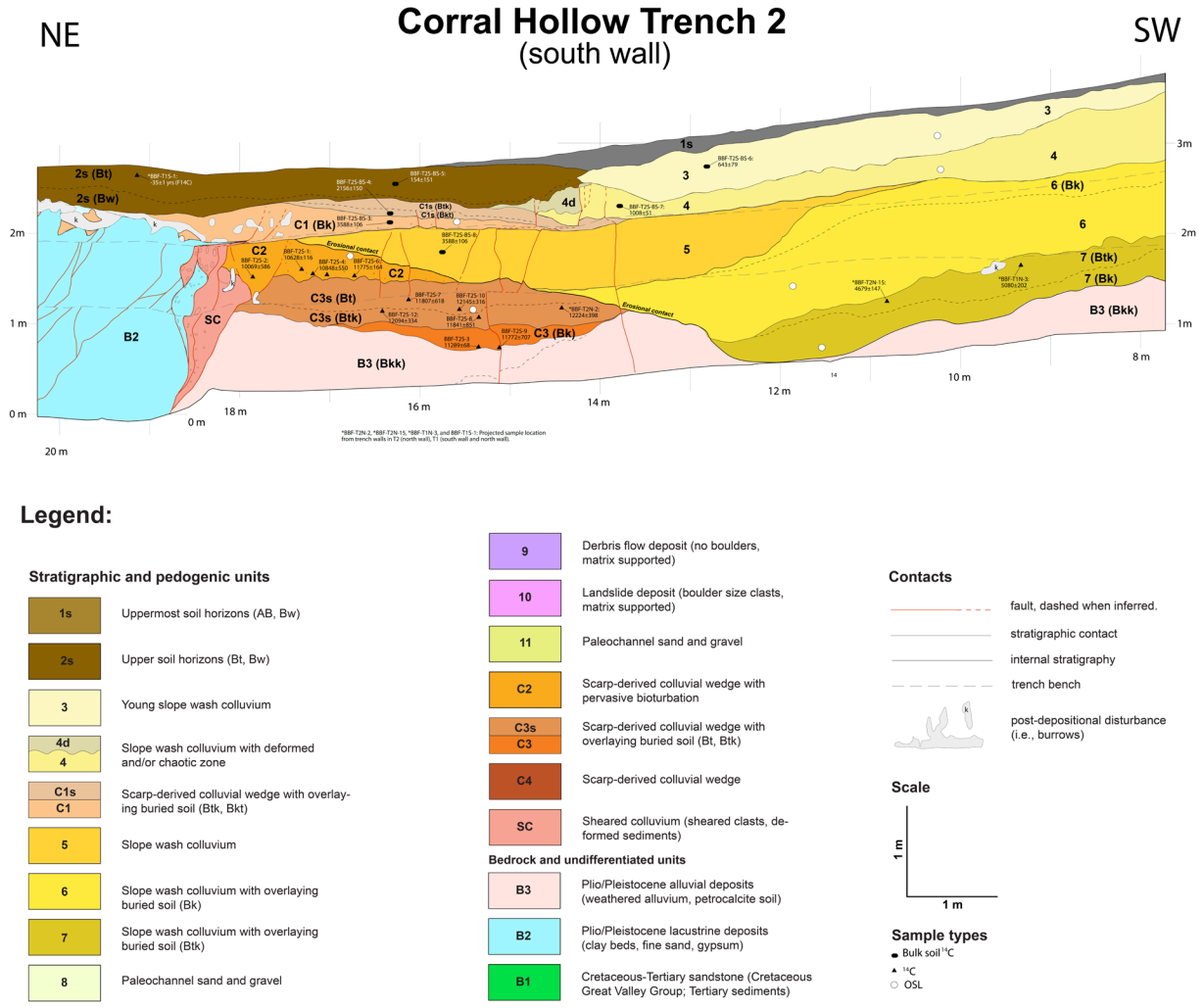

Figure 7. Stratigraphic and structural relations for Trench 2 south wall showing radiocarbon ages. See Table 1 and Figure 8 for sample info and age results.

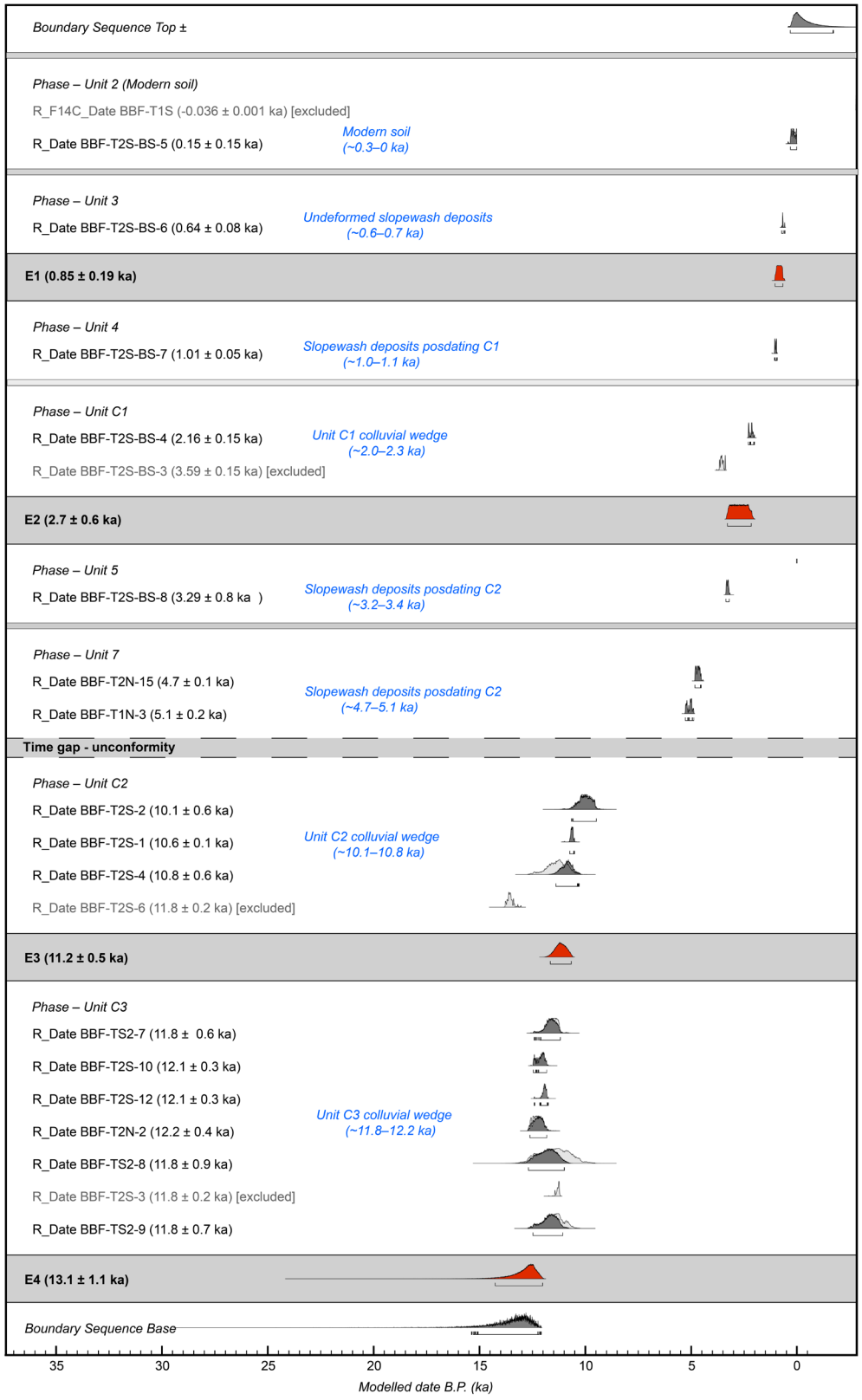

Figure 8. Bayesian (OxCal) model for the Corral Hollow paleoseismic trench site, showing stratrigrapohic ordering and geochronologic results from T1 and T2.

7. CONCLUSION

New understanding of the earthquake occurrence and seismotectonics of the Black Butte-San Joaquin fault system provides constraints of the potential earthquake hazards to the Sacramento–San Joaquin Delta region. Our Corral Hollow earthquake chronology on the Black Butte fault indicate evidence of at least four surface rupturing earthquakes since ~13 ka. OxCal Bayesian modeling of 20 radiocarbon ages constrained the timing of earthquakes E1−E4 in context of stratigraphic and structural relations of fault-scarp derived colluvial wedges. Black Butte fault earthquakes occurred at ~1 ka (E1), ~ 3 ka (E2), ~11 ka (E3), and ~13 ka (E4). Time intervals between earthquakes range from ~2 ka to ~8 ka. Given, the possibility that one or more earthquakes may have occurred during a ~ 5-kyr period associated with an unconformity, a shorter average recurrence interval of ~2 ka seems likely. We speculate that 1−2 additional earthquakes may have occurred sometime between E3 and E2, based on an unconformity between 10.1−10.8 ka and 4.7−5.1 ka. A vertical slip deficit of ~1.1 m since the last earthquake (ca. 1 ka) suggest multiple earthquakes or a single large event are needed to relieve accumulated strain via ~0.4 m slip-per event. Our estimate of vertical slip-per event lower than the inferred slip deficit from the loading rate could also result from highly variable slip distribution, incomplete paleoseismic record, or increase strain partitioning via strike-slip deformation during the Holocene.

Our results indicate the Black Butte–San Joaquin faults system is a seismogenic source to the FSacramento–San Joaquin Delta with the potential to generate significant surface rupturing earthquakes. This study builds on the previous NEHRP-funded work by Gavillot and Meigs (2020) that sought to reevaluate existing regional seismic source models for Sacramento–San Joaquin Delta. Our findings reinforce the need to include Black Butte–San Joaquin faults system in future updates to seismic hazard assessments used in the Northern California Community Fault Model, UCERF, National Seismic Hazards Model (NSHM), and Delta Risk Management (DRMS) for the Sacramento-San Joaquin Delta and its infrastructure.

Acknowledgments. This material is based upon work supported by the U.S. Geological Survey under Grant No. G20AP00078 and received collaborative support from the U.S. Geological Survey Earthquake Science Center in the research activities of seismic hazards in the Sacramento–San Joaquin Delta. We would like to particularly thank Stephen DeLong, Alexandra Pickering, Robert Sickler, and Suzanne Hecker that have collaborated in the field data collection and age analyses. We would like to thank Susan Zimmerman at Lawrence Livermore National Laboratory and Linda Cummings at PaleoReserach Institute for processing the radiocarbon age results. We thank Shannon Mahan at the USGS Luminescence Lab for processing the IRSL samples. We thank fruitful discussions and trench reviews from Janet Sowers, Chris Madugo, Tim Dawson, John Baldwin, Gordon Seitz, Ozgur Kozaci "Oz", and Donald Wells. We also thank field assistance from Joanna Gavillot, Garret Huddleston, and Danielle Madugo. We thank Contra Costa Water District-Los Vaqueros Watershed for providing access to the trench site and making this study possible.

References

Bronk Ramsey, C, 1995, Radiocarbon calibration and analysis of stratigraphy: The OxCal program, Radiocarbon, 37 (2) 425-430

Bronk Ramsey, C., 2009, Bayesian Analysis of Radiocarbon Dates. Radiocarbon, 51, 337-360. https://doi.org/10.1017/S0033822200033865

d'Alessio, M.A., Johanson, I.A., Bürgmann, R, Schmidt, D.A., and M.H. Murray, 2005, Slicing up the San Francisco Bay Area: Block kinematics and fault slip rates from GPS-derived surface velocities. Journal of Geophysical Research 110, doi:10.1029/2004JB003496.

Dibblee, T.W., Jr., 1981a, Preliminary geologic map of the Lone Tree Creek quadrangle, San Joaquin and Stanislaus Counties, California: United States Geological Survey Open-File Report 81-466, scale 1:24,000.

Dibblee, T.W., Jr., 1981b, Preliminary geologic map of the Tracy quadrangle, San Joaquin County, California: United States Geological Survey Open-File Report 81-464, scale 1:24,000.

Field, E.H., Biasi, G.P., Bird, P., Dawson, T.E., Felzer, K.R., Jackson, D.D., Johnson, K.M., Jordan, T.H., Madden, C., Michael, A.J., Milner, K.R., Page, M.T., Parsons, T., Powers, P.M., Shaw, B.E., Thatcher, W.R., Weldon, R.J., II, and Zeng, Y., 2013, Uniform California earthquake rupture forecast, version 3 (UCERF3)—The time-independent model: U.S. Geological Survey Open-File Report 2013–1165, 97 p., California Geological Survey Special Report 228, and Southern California Earthquake Center Publication 1792, http://pubs.usgs.gov/of/2013/1165/.

Gavillot, Y.G., DeLong, S., Pickering, A., Cyr, A., and Meigs, A., 2018, Reevaluating seismic hazards from new mapping of the Back Butte-San Joaquin fold-thrust belt, Sacramento-San Joaquin Delta, Abstract # 457459, American Geophysical Union Fall Meeting, Washington, D.C., 10–14 Dec. 2018.

Gavillot, Y.G., and Meigs, A., 2020, Deformation rates, detailed mapping, and seismic hazard of the Black Butte–San Joaquin fold and thrust belt adjacent to the Sacramento–San Joaquin Delta: Collaborative Research with Oregon State University and the U.S. Geological Survey: National Earthquake Hazards Reduction Program Award Number, Final Technical Report – G18AP00093

Guzofski, C.A., Shaw, J.H., Lin, G., and Shearer, P.M., 2007, Seismically active wedge structure beneath the Coalinga anticline, San Joaquin basin, California, J. Geophys. Res., 112, B03S05, doi:10.1029/2006JB004465.

Jennings, C.W., 1994, Fault activity map of California and adjacent areas: California Department of Conservation, Division of Mines and Geology, Geologic Data Map No. 6, scale 1:750,000.

Jennings, C.W. and Bryant, W.A., 2010, Fault activity map of California: California Geological Survey Geologic Data Map No. 6.

Krug, E.H., Cherven, V.B., Hatten, C.W., and Roth, J.C., 1992, Subsurface structure in the Montezuma Hills, southwestern Sacramento basin, in Cherven, V.B., and Edmondson, W.F., eds., Structural Geology of the Sacramento Basin: Volume MP-41, Annual Meeting, Pacific Section, Society of Economic Paleontologists and Mineralogists, p. 41-60.

Lettis, W.R., 1982, Late Cenozoic stratigraphy of the western margin of the central San Joaquin Valley, California: U.S. Geological Survey Open-File Repot 82-526, 203 p., scale 1:24,000.

Lettis, W.R., and Unruh, J.R., 1991, Quaternary geology of the Great Valley, California: in Morrison, R.B., ed., Quaternary non-glacial geology of the conterminous United States: Boulder, Colorado, Geological Society of America, Decade of North American Geology, v. K2.

Noller, J.S., Sowers, J.M., and Lettis, W.R., 1993, Quaternary geology of the Solyo and LoneTree Creek 7.5-minute quadrangles, California: U.S. Geological Survey Open File Report 93 224.

O'Connell, D. R., Unruh, J. R. and Block, L. V., 2001, Source Characterization and Ground-Motion Modeling of the 1892 Vacaville–Winters Earthquake Sequence, California, Bulletin of the Seismological Society of America, v. 91, no.6, p. 1471-1497.

Page, M.T., Field, E. H., Milner, K.R., and Powers, P.M, 2013, Appendix N—Grand Inversion Implementation and Testing in Field, E. H and others, 2013, Uniform California earthquake rupture forecast, version 3 (UCERF3)—The time-independent model: U.S. Geological Survey Open-File Report 2013–1165, 97 p., California Geological Survey Special Report 228, and Southern California Earthquake Center Publication 1792, http://pubs.usgs.gov/of/2013/1165/.

Prescott, W.H., Savage, J.C., Svarc, J.L., and Manaker, D., 2001, Deformation across the Pacific-North American plate boundary near San Francisco, California: Journal of Geophysical Research, v. 106, no. B4, p. 6673-6682.

Real, C.R. and Knudsen, K.L., 2010, Application of New Liquefaction Hazard Mapping Techniques to the Sacramento-San Joaquin Delta Area: Collaborative Research with URS Corporation and California Geological Survey: Final Technical Report, U.S. Geological Survey, National Earthquake Hazards Reduction Program, Award Number 08HWGR0092-93, 56p.

Rittenour, T.M., 2008, Luminescence dating of fluvial deposits: Applications to geomorphic, paleoseismic and archaeological research: Boreas, v. 37, p. 613–635, doi:10.1111/j.1502-3885.2008.00056.x.

Rhodes, E.J., 2011, Optically stimulated luminescence dating of sediments over the past 200,000 years: Annual Review of Earth and Planetary Sciences, v. 39, p. 461– 488, doi:10.1146/annurev-earth-040610-133425.

Sowers, J.M., Sharp, W. D., Southard, R. J., and Ludwig, K. R., 2000, Quaternary deformation along East Front of the Diablo Range near Tracy, CA: U. S. Geological Survey, National Earthquake Hazards Reduction Program, Final Technical Report 99-HQ-GR-0101.

Sterling, R., 1992, Intersection of the Stockton and Vernalis faults, southern Sacramento Valley, California, in Chervon, V.B., and Edmondson, W.F., eds, Structural Geology of the Sacramento Basin: American Association of Petroleum Geologists Miscellaneous Publication 41, Pacific Section, p. 143-151.

Stuiver, M., and Polach, H., 1977, Discussion: Reporting of 14C Data. *Radiocarbon*, 19, 355-363.

Unruh, J.R. and Sawyer, T.L., 1995, Late Cenozoic growth of the Mt. Diablo fold and thrust belt, central Contra Costa County, California, and implications for transpressional deformation of the northern Diablo Range [abs.]: American Association of Petroleum Geologists, 1995 Pacific Section Convention Abstracts, 47 p.

Unruh, J.R. and Hector, S., 1999, Subsurface characterization of the Potrero-Ryer Island Thrust System, western Sacramento-San Joaquin Delta, northern California: Final Technical Report, U.S. Geological Survey, National Earthquake Hazards Reduction Program Award Number, Award Number 1432-HQ-96-GR-02724, 34p.

Unruh, J.R and Krug, K., 2007, Assessment and Documentation of Transpressional Structures, Northeastern Diablo Range, for the Quaternary Fault Map Database: Collaborative Research with William Lettis & Associates, Inc., and the U.S. Geological Survey: U. S. Geological Survey, National Earthquake Hazards Reduction Program Award Number, Final Technical Report - 06HQGR0139.

Unruh, J.R., Hitchcock, C.S., Hector, S., and Blake, K., 2009, Characterization of Potential Seismic Sources in the Sacramento-San Joaquin Delta, California: Final Technical Report, U.S. Geological Survey, National Earthquake Hazards Reduction Program Award Number, Award Number 08HQGR0055, 45p.

Unruh, J.R. and Hitchcock, C.S., 2015, Detailed Mapping and Analysis of Fold Deformation Above the West Tracy Fault, Southern San Joaquin-Sacramento Delta, Northern California: Collaborative Research with Lettis Consultants International and InfraTerra: U. S. Geological Survey, National Earthquake Hazards Reduction Program Award Number, Final Technical Report – G14AP00069

Wells, D. L. and Coppersmith, K. J., 1994, New empirical relationships among magnitude, rupture length, rupture width, rupture area, and surface displacement: Bulletin of the Seismological Society of America, v. 84, no. 4, p. 974-1002.

Witter, R.C., Knudsen, K.L., Sowers, J.M., Wentworth, C.M., Koehler, R.D., Randolph, C.E., 2006, Maps of Quaternary Deposits and Liquefaction Susceptibility in the Central San Francisco Bay Region, California: U.S. Geological Survey, Open-File Report 2006-1037.